AIAA JOURNAL
Vol. 38, No. 9, September 2000

Numerical Solution of the Reduced Navier–Stokes Equations for Internal Incompressible Flows

Martin Scholtysik,* Bernhard Müller,† and Torstein K. Fanneløp‡
Swiss Federal Institute of Technology, CH-8092 Zürich, Switzerland

A space-marching method is developed to solve a reduced (parabolized) form of the three-dimensional steady Navier–Stokes equations for internal incompressible flows. Finite differences and a collocated variable arrangement are used to discretize the equations. The single-pass version of the method involves an approximation of the streamwise pressure gradient and computes the entire flowfield with only one pass through the spatial domain. The multiple-pass version needs to store the complete three-dimensional pressure field but does not approximate the streamwise pressure gradient. A new scheme to solve the incompressible Navier–Stokes equations is introduced that combines a high-order upwind formulation with the concept of a pressure-correction equation. In this approach, denoted artificial pressure diffusion (APD), the time derivative of the Laplacian of the pressure is introduced in the continuity equation. The modified continuity equation and the unsteady momentum equations can be solved either with the segregated approach similar to the SIMPLEC method or the fully coupled approach similar to the artificial compressibility method. The new computer code is verified on several test cases including the two-dimensional driven-cavity test case at $Re = 1.0 \times 10^4$. The method is applied to the turbulent flow in the boundary-layer channel of the Institute of Fluid Dynamics at the Swiss Federal Institute of Technology to investigate the effect of lateral flow convergence/divergence. The solution is compared to experimental data and other numerical solutions.

I. Introduction

THE main objective of the present work is the development of a computational method to predict internal incompressible flows accurately and efficiently with the help of a reduced set of the Navier–Stokes equations. The method should be able to predict slender internal flows more accurately than the solution to the boundary-layer equations, but with less effort than required for the full Navier–Stokes equations.

The turbulent high-Reynolds-number flow in the boundary-layer channel (BLC) of the Institute of Fluid Dynamics at the Swiss Federal Institute of Technology (ETH Zürich) is analyzed with the new method. The channel was designed to investigate the effect of lateral convergence/divergence of the streamlines at the edge of the boundary layer in the absence of a streamwise pressure gradient. Depending on the chosen flow direction, the three-dimensional nozzle shown in Fig. 1 can be used to generate either convergent (case 3Dc) or divergent external streamlines (case 3Dd). The two-dimensional reference nozzle (case 2Dz) generates a flow with parallel external streamlines. Pompeo[1] carried out experimental investigations that were published together with two-dimensional computations of the floor boundary layer in the plane of symmetry.[2] The solution of the first-order boundary-layer equations in streamline coordinates for the cases 2Dz and 3Dd were satisfactory within the expected accuracy of the simple turbulence model, but the case 3Dc led to diverging solutions. Also, only a small part of the flowfield could be computed as no lateral boundary conditions could be used. In contrast, the measurements did not show any kind of irregularity or diverging behavior. Thomann[3] identified the problem as a singularity of the three-dimensional boundary-layer equations for the case of convergent external streamlines. Scholtysik et al.[4] confirmed his results with a stability analysis, showing different sensitivities for flows with convergent and divergent external streamlines.

Received 4 December 1998; revision received 17 September 1999; accepted for publication 6 October 1999.

*Research Scientist, Institute of Fluid Dynamics; currently Application Engineer, SULZER TURBO Ltd., CH-8023 Zürich, Switzerland.

†Assistant Professor, Institute of Fluid Dynamics; currently Lecturer, Department of Scientific Computing, Uppsala University, S-75104 Uppsala, Sweden.

‡Professor and Head (retired), Institute of Fluid Dynamics; current address: Utsikten 6, N-3155 Asgaardstrand, Norway. Member AIAA.

A. Space-Marching Methods

The development of a flow through a slender channel depends mainly on geometry and upstream conditions. This type of flow can be predicted with a space-marching method. Not all data of the complete flowfield have to be kept in memory, but only a smaller set for the surfaces orthogonal to the main flow direction (crossflow surfaces). Hence, a substantial reduction of the required computer memory and a finer resolution of the flowfield can be achieved for a given computer. There is no restriction on the flow in the crossflow directions (secondary flow); even recirculation and separation are allowed. Three mechanisms can propagate influences against the predominant flow direction: recirculation, pressure transmission, and viscous diffusion. They can lead to a breakdown of the solution (departure solution) if not treated properly. For high-Reynolds-number flows viscous diffusion in the streamwise direction can be neglected without introducing large errors (Ref. 5, Chap. 8).

Several reduced forms of the Navier–Stokes equations are found in the literature, e.g., the parabolized Navier–Stokes equations (PNS) and the partially parabolized Navier–Stokes equations (PPNS). Different approaches are used to compute the streamwise pressure gradient and to treat areas of recirculation. For subsonic flows the streamwise pressure gradient has to be forward differenced to get a stable marching method, but the downwind pressure is unknown a priori. In a PPNS method the solution is obtained by repeated passes through the computational domain. Only the pressure is stored in a complete three-dimensional array. Kirtley and Lakshminarayana[6] used a multiple-pass method to compute the PPNS equations. The number of global iterations is comparatively high (up to 200), resulting in computing times similar to efficient conventional full Navier–Stokes computations. In a PNS method the solution is obtained with a single pass through the computational domain. Patankar and Spalding[7] split the pressure into two independent parts. The first part gives the variation in the crossflow surface and is determined by the continuity equation. The second part represents the pressure drop caused by the viscous resistance on the boundaries and the axial acceleration caused by changes of the cross-sectional area. It is determined from the conservation of mass flow in the channel. Briley[8] added a third contribution to the pressure. This part represents the elliptic effects in the pressure field, and it is treated as a source term. Briley and McDonald[9] presented a more complicated approach, in which the transverse velocity vector that corrects a given potential flow is decomposed into potential and rotational vector components. Aslan[10] solved the compressible

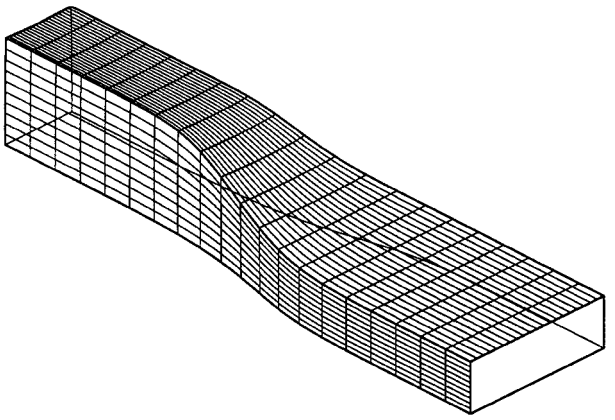

Fig. 1 Three-dimensional nozzle of the BLC.

PNS equations with a segregated marching procedure. The pressure is determined from a pressure equation similar to the SIMPLER method. The momentum equations are transformed to a set of three equations for the contravariant velocity components. This formulation allows the streamwise and crossflow velocity components to be solved separately. A review of the computational techniques for solving reduced/parabolized forms of the Navier–Stokes equations is given by Rubin and Tannehill.[11] More detailed information is given in the textbooks by Anderson et al.,[5] Fletcher,[12] and Hirsch.[13]

B. Methods for Incompressible Flows

As the density variation in the BLC is below 1% (experiments of Pompeo[1,2]), the density is assumed to be constant in the present work. The flow equations on a crossflow surface can be interpreted as the full two-dimensional Navier–Stokes equations with additional terms arising from the third (marching) direction. As no terms are neglected in the crossflow directions, some methods for solving the two-dimensional Navier–Stokes equations can be modified to solve the three-dimensional PNS equations.

Chorin[14] proposed the so-called artificial compressibility method. It can be considered as a typical example of a *coupled approach*. The continuity equation is modified by adding the time derivative of the pressure. This allows a development of the solution by time stepping. In steady state the time derivative of the pressure vanishes, and the correct continuity and momentum equations are now satisfied up to machine accuracy. Because the modified continuity equation and the unsteady inviscid momentum equations form a hyperbolic system, numerical methods for hyperbolic systems can be applied as for the compressible Euler equations. Rogers and Kwak[15] used a coupled approach with a higher-order upwind discretization of the inviscid fluxes including the pressure and a second-order central discretization of the viscous fluxes. Abdallah[16,17] and Sotiropoulos and Abdallah[18] presented a series of publications on a coupled approach in which the continuity equation is replaced by a Poisson equation for the pressure. The authors report good convergence properties because of the dissipative nature of the Poisson operator. However, the continuity equation can be satisfied only up to a small error to ensure a smooth solution of the pressure. Dick[19] suggested a coupled approach for steady flows. In this method the continuity and momentum equations are used in their steady-state form. Using Newton's method, the system of equations is advanced iteratively from an initial guess.

The SIMPLE method can be seen as a typical example of a *segregated approach*. The method was proposed by Patankar and Spalding[7] in a finite volume formulation on a staggered grid and served as a base for further variants as SIMPLEC[20] and SIMPLER.[21] This family of schemes has been used for many practical applications in the last 20 years. A comparison of different variants is given by Raithby and Schneider.[22] Rodi et al.[23] presented a survey on computational methods for complex, incompressible flows. The book edited by Gunzburger and Nicolaides[24] describes recent approaches to solve the incompressible Navier–Stokes equations.

C. Odd-Even Decoupling

Some of the methods just mentioned can produce oscillatory solutions for pressure and velocity. Artificial viscosity on all variables can prevent the growth of oscillations but introduces errors in the solution. As an alternative, upwind schemes suppress oscillations by the use of noncentered computational stencils. Here, higher-order formulations are required to reduce the amount of numerical dissipation. If the upwind formulation is applied only to the convective terms and does not include the pressure gradient, the pressure can still exhibit oscillatory solutions as reported by Rhie and Chow.[25] The staggered grid is a remedy used to avoid these pressure oscillations. Peric et al.[26] presented a comparison between a staggered and a collocated arrangement. They find little differences in accuracy or convergence of the two formulations. However, they prefer the collocated arrangement, as the treatment of the geometry and the boundary conditions as well as the implementation of higher-order differencing schemes become simpler. Rhie and Chow[25] published a method denoted momentum interpolation. In this method a special interpolation procedure for evaluating the fluxes at cell faces is used to avoid the nonphysical oscillations. Majumdar et al.[27] use this method in combination with an upwind method for the velocity. A promising approach has been presented by Hayase et al.[28] They construct a consistent variant of the QUICK scheme using a third-order upwind formulation for the momentum equations. The pressure is computed on a staggered grid using the SIMPLER method. Yoon and Kwak[29] proposed a flux-limited dissipation model with scalar coefficients. This model is a practical alternative to the more expensive upwind schemes. Tafti[30] uses a third-order forward-biased (or backward-biased) operator for the pressure gradient on a collocated grid. The same operator is used also to express the Laplacian in the pressure equation.

D. Present Method

The PNS and PPNS equations for a steady incompressible flow were chosen as governing equations. The complete cross section of the channel is solved, and the no-slip condition for velocity is enforced at the wall. A finite difference formulation and a collocated variable arrangement on a structured grid are chosen. This allows an efficient clustering of grid points in regions of large gradients at the walls. The effect of turbulence is modeled with the simple algebraic Baldwin–Lomax[31] turbulence model. The results presented here are obtained with two different but related methods. The single-pass method (SPM) and the multiple-pass method (MPM) differ primarily in the treatment of the pressure gradient term in the main flow direction. For the formulation of the SPM, the concept of Briley[8] is used, employing an approximation for the streamwise pressure gradient. The MPM does not use an approximation of the streamwise pressure gradient. This method performs repeated passes through the spatial domain improving the three-dimensional pressure field with every pass.

For the solution of a crossflow surface, a new scheme termed *artificial pressure diffusion* (APD) is presented to drive the solution from an initial guess to the steady state. The continuity equation is modified in the spirit of a Poisson equation for the pressure corrections. As only a time derivative of the Laplacian of the pressure is added, the steady-state result is not affected by the modification. The fifth-order upwind formulation used by Rogers and Kwak[15] is used to avoid odd-even decoupling without introducing excessive dissipation. The upwind scheme includes the convective and the pressure-gradient terms as well as the continuity equation. The APD method can solve the governing equations as a coupled or a segregated procedure. In the segregated approach a Poisson equation is used to compute the pressure corrections, similar to the SIMPLEC method. In the coupled approach the coupling of continuity and momentum equations is automatically achieved by the implicit solution procedure. As the same spatial discretization is used for the coupled and the segregated procedure, they converge to the same solution up to machine accuracy.

II. Numerical Method

The continuity and momentum equations are written in terms of nondimensional variables, using a reference length l_0, velocity v_0, density ρ_0, and kinematic viscosity ν_0.

$$\operatorname{div} \boldsymbol{v} = 0 \tag{1}$$

$$\boldsymbol{v} \cdot \operatorname{grad} \boldsymbol{v} = -\operatorname{grad} p + (1/Re) \operatorname{div}\{\nu[\operatorname{grad} \boldsymbol{v} + (\operatorname{grad} \boldsymbol{v})^T]\} \tag{2}$$

The Reynolds number is formed with these reference values as $Re = v_0 l_0 / \nu_0$. The static pressure is divided by $v_0^2 \rho_0$ and henceforth referred to as pressure p. In Cartesian coordinates the nondimensional velocity $\boldsymbol{v}$ has components u, v, w. For laminar flows the nondimensional kinematic viscosity ν equals unity. For turbulent flows the dependent variables represent the mean values of the flow, and the effect of turbulence is modeled as an eddy viscosity ν_t using the algebraic turbulence model of Baldwin and Lomax.[31] The model modification used to compute three-dimensional corner flows is given by Scholtysik.[32]

A coordinate transformation is introduced as described by Anderson et al.[5] (pp. 252–255 and 430–433). The Cartesian coordinates (x, y, z) in the physical domain are transformed to the computational domain by a transformation of the form $\xi = \xi(x, y, z)$, $\eta = \eta(x, y, z)$, $\zeta = \zeta(x, y, z)$. The metrics and the Jacobian determinant of the transformation are formed as

$$\xi_x = J(y_\eta z_\zeta - y_\zeta z_\eta), \qquad \eta_x = -J(y_\xi z_\zeta - y_\zeta z_\xi)$$

$$\zeta_x = J(y_\xi z_\eta - y_\eta z_\xi)$$

$$\xi_y = -J(x_\eta z_\zeta - x_\zeta z_\eta), \qquad \eta_y = J(x_\xi z_\zeta - x_\zeta z_\xi)$$

$$\zeta_y = -J(x_\xi z_\eta - x_\eta z_\xi)$$

$$\xi_z = J(x_\eta y_\zeta - x_\zeta y_\eta), \qquad \eta_z = -J(x_\xi y_\zeta - x_\zeta y_\xi)$$

$$\zeta_z = J(x_\xi y_\eta - x_\eta y_\xi) \tag{3}$$

$$J^{-1} = x_\xi(y_\eta z_\zeta - y_\zeta z_\eta) - x_\eta(y_\xi z_\zeta - y_\zeta z_\xi) + x_\zeta(y_\xi z_\eta - y_\eta z_\xi) \tag{4}$$

The terms x_ξ, x_η, etc., are computed from the coordinates of the grid points with an averaging procedure introduced by Pulliam and Steger[33] to ensure freestream preservation. The contravariant velocity components are

$$U_c = u\xi_x + v\xi_y + w\xi_z, \qquad V_c = u\eta_x + v\eta_y + w\eta_z$$

$$W_c = u\zeta_x + v\zeta_y + w\zeta_z \tag{5}$$

The continuity and momentum equations can be written in divergence form as one system of equations introducing the convective, pressure, and viscous fluxes

$$\frac{\partial \boldsymbol{E}}{\partial \xi} + \frac{\partial \boldsymbol{F}}{\partial \eta} + \frac{\partial \boldsymbol{G}}{\partial \zeta} = 0, \qquad \begin{aligned} \boldsymbol{E} &= \boldsymbol{E}_c + \boldsymbol{E}_p - \boldsymbol{E}_v \\ \boldsymbol{F} &= \boldsymbol{F}_c + \boldsymbol{F}_p - \boldsymbol{F}_v \\ \boldsymbol{G} &= \boldsymbol{G}_c + \boldsymbol{G}_p - \boldsymbol{G}_v \end{aligned} \tag{6}$$

$$\boldsymbol{E}_c = (U_c/J)[1, u, v, w]^T, \qquad \boldsymbol{F}_c = (V_c/J)[1, u, v, w]^T$$

$$\boldsymbol{G}_c = (W_c/J)[1, u, v, w]^T \tag{7}$$

$$\boldsymbol{E}_p = (p/J)[0, \xi_x, \xi_y, \xi_z]^T, \qquad \boldsymbol{F}_p = (p/J)[0, \eta_x, \eta_y, \eta_z]^T$$

$$\boldsymbol{G}_p = (p/J)[0, \zeta_x, \zeta_y, \zeta_z]^T \tag{8}$$

$$\boldsymbol{F}_v = \frac{1}{ReJ}\left(\eta_x \begin{bmatrix} 0 \\ \tau_{xx} \\ \tau_{yx} \\ \tau_{zx} \end{bmatrix} + \eta_y \begin{bmatrix} 0 \\ \tau_{xy} \\ \tau_{yy} \\ \tau_{zy} \end{bmatrix} + \eta_z \begin{bmatrix} 0 \\ \tau_{xz} \\ \tau_{yz} \\ \tau_{zz} \end{bmatrix}\right)$$

$$\boldsymbol{G}_v = \frac{1}{ReJ}\left(\zeta_x \begin{bmatrix} 0 \\ \tau_{xx} \\ \tau_{yx} \\ \tau_{zx} \end{bmatrix} + \zeta_y \begin{bmatrix} 0 \\ \tau_{xy} \\ \tau_{yy} \\ \tau_{zy} \end{bmatrix} + \zeta_z \begin{bmatrix} 0 \\ \tau_{xz} \\ \tau_{yz} \\ \tau_{zz} \end{bmatrix}\right) \tag{9}$$

with the nondimensional viscous stress tensor $\tau = \nu[\operatorname{grad} \boldsymbol{v} + (\operatorname{grad} \boldsymbol{v})^T]$, as for example given by Anderson et al.[5] (p. 186). The PPNS equations are obtained by neglecting the viscous flux $\boldsymbol{E}_v$ in the marching direction and by neglecting all ξ derivatives in the viscous stress tensor. The vector of the unknown is $\boldsymbol{Q} = [p, u, v, w]^T$.

A. SPM

Spatial marching is possible if no information is allowed to propagate against the marching direction, which is ensured by two approximations—one on the viscous terms as just introduced for the PPNS equations and one on the pressure. The pressure is split into three parts as proposed by Briley[8]:

$$p = p_{\mathrm{cl}}(\xi) + p_v(\xi, \eta, \zeta) + p_i(\xi, \eta, \zeta) \tag{10}$$

where $p_{\mathrm{cl}}(\xi)$ is the pressure on the centerline. The part $p_v(\xi, \eta, \zeta)$ is the pressure from viscous effects. It is computed from the local divergence of the velocity and acts only in the crossflow directions. The part p_v of the pressure is computed independently for every crossflow surface, and the viscous part of the streamwise pressure gradient $\partial p_v / \partial \xi$ is neglected. The part $p_i(\xi, \eta, \zeta)$ is the pressure from inviscid or elliptic effects. It has to be prescribed, e.g., as the potential solution, and cannot be computed as part of the marching solution.

The solution for a crossflow surface is obtained with an iteration in two steps. In the first step the velocity $\boldsymbol{v}$, the viscous pressure p_v, and the volume flow $\dot{V}$ in the channel are computed for a crossflow surface, using the pressure gradient on the centerline $\partial p_{\mathrm{cl}} / \partial \xi$ of the preceding iteration. In the second step $\partial p_{\mathrm{cl}} / \partial \xi$ is adjusted to establish a constant volume flow in the channel. To derive an iterative correction procedure for $\partial p_{\mathrm{cl}} / \partial \xi$, a streamline of an inviscid flow is considered. Bernoulli's law is linearized for small changes in velocity, giving a relation between pressure and velocity changes on the streamline as $\mathrm{d}p \approx -\bar{u}_{\mathrm{CS}}\, \mathrm{d}u$. The pressure gradient on the centerline $\partial p_{\mathrm{cl}} / \partial \xi$ at the new iteration level $n + 1$ is adjusted in order to compensate for the remaining error in the volume flow as

$$\left(\frac{\mathrm{d}p_{\mathrm{cl}}}{\mathrm{d}\xi}\right)^{n+1} = \left(\frac{\mathrm{d}p_{\mathrm{cl}}}{\mathrm{d}\xi}\right)^{n} + \bar{u}_{\mathrm{CS}} \frac{(\dot{V}^n - \dot{V}|_{\mathrm{inlet}})}{A_{\mathrm{CS}}} \tag{11}$$

where $\bar{u}_{\mathrm{CS}}$ is taken as the average velocity on the crossflow surface and A_{CS} denotes its area.

B. MPM

The viscous diffusion in the marching direction is neglected, although all terms of the three-dimensional Navier–Stokes equations could be retained in principle. No approximation is introduced for the pressure-gradient term, and the pressure is not split. The downwind pressure is taken from the previous sweep through the domain. This requires the storage of the entire three-dimensional pressure field. To stabilize the entire procedure, only a part of the computed changes is added to the preceding solution. The fastest convergence of the overall method is observed when the domain is swept alternately in the streamwise and upstream direction, once carrying the inflow information down to the end of the channel and once carrying the pressure information toward the inlet. For an upstream sweep the velocity in front of the crossflow surface has to be known, requiring the storage of the entire three-dimensional velocity field.

C. APD

The solution process of one crossflow surface (SPM and MPM) can be interpreted as the solution of the full two-dimensional Navier–Stokes equations with source terms made up by the derivatives in the marching direction. A new scheme for the solution of the incompressible Navier–Stokes equations, which combines the upwind model of Rogers and Kwak[15] with the concept of a pressure-correction equation, is presented here. The time derivative of a Laplacian operator of the pressure is added in the continuity equation (1)

$$-(F_{\mathrm{APD}}\, \mathrm{d}t) \frac{\partial(\nabla^2 p)}{\partial t} + \operatorname{div} \boldsymbol{v} = 0 \tag{12}$$

This leads to a desired diffusivity in solution process (APD). In the steady state the time derivative vanishes, and the unmodified continuity equation is solved up to machine accuracy. In a similar way as Chorin's artificial compressibility method generalizes the penalty method, the APD method may be viewed as a generalization

of the ansatz $-\varepsilon\nabla^2 p + \operatorname{div} \boldsymbol{v} = 0$ used by Rannacher.[34] Two different variants are described here: the first following a segregated approach and the other a fully coupled one. In both methods the change of pressure over one time (or iteration) step can be expressed as p'

$$-F_{\mathrm{APD}}\nabla^2 p' + \operatorname{div} \boldsymbol{v} = 0 \tag{13}$$

In the segregated approach p' is computed from the pressure correction equation, and in the coupled approach p' is the change of pressure over one iteration step (δp). The coefficient F_{APD} is chosen differently for the segregated and the coupled approach. The characteristics of both methods are summarized here. For the segregated approach these are the characteristics:

1) The Poisson term is needed to couple the continuity and momentum equations.

2) $F_{\mathrm{APD}} = \mathrm{d}t$.

3) The velocity at the new time level is divergence free in the discrete sense.

4) A corrective velocity u' is computed from the pressure corrections p'.

5) $\operatorname{div} \boldsymbol{v}$ is evaluated at the old level n.

For the coupled approach these are the characteristics:

1) The Poisson term acts as an artificial dissipation and relaxes the incompressibility constraint.

2) $F_{\mathrm{APD}} = \text{constant}$.

3) The velocity at the new time level is not divergence free (for nonzero F_{APD}).

4) All changes ($\delta \boldsymbol{Q}$) are computed by the implicit scheme. Additional corrections u' to the velocity are not required.

5) $\operatorname{div} \boldsymbol{v}$ is evaluated at the new level $n + 1$.

D. Segregated Approach

In the segregated approach the continuity and momentum equations are solved iteratively in two steps. In the first step only the momentum equations are advanced with an explicit time-stepping procedure without considering the continuity equation. Therefore, the continuity equation is not satisfied at the end of this step unless the steady state is reached. In a second step corrective pressure and velocity fields are computed to satisfy the continuity equation. The unsteady form of the momentum equations is used to formulate a time-marching procedure

$$\frac{\partial \boldsymbol{v}}{\partial t} = -\operatorname{grad} p - \boldsymbol{v} \cdot \operatorname{grad} \boldsymbol{v} + \frac{1}{Re} \operatorname{div}\{\nu[\operatorname{grad} \boldsymbol{v} + (\operatorname{grad} \boldsymbol{v})^T]\} \tag{14}$$

The flow variables $\boldsymbol{v}$, p, and ν are split into provisional quantities computed in the first step (superscript *) and corrective quantities in the second step (superscript $'$). At the new time level the flow variables are $\boldsymbol{v}^{n+1} = \boldsymbol{v}^* + \boldsymbol{v}'$, $p^{n+1} = p^* + p'$, and $\nu^{n+1} = \nu^* + \nu'$. The unmodified continuity equation becomes $\operatorname{div} \boldsymbol{v}^{n+1} = \operatorname{div} \boldsymbol{v}^* + \operatorname{div} \boldsymbol{v}' = 0$. The right-hand side of the momentum equation is evaluated at the old time level n, and the provisional values $\boldsymbol{v}^*$ are computed with an explicit Euler discretization of the time derivative $\partial \boldsymbol{v}/\partial t = (\boldsymbol{v}^* - \boldsymbol{v}^n)/\mathrm{d}t$. The resulting explicit scheme can easily be solved for $\boldsymbol{v}^*$, but the time-step limitation prevents a fast overall convergence in regions of small grid spacings. The efficiency of the method can be improved with an iterative residual smoothing.

In the second step a corrective velocity field $\boldsymbol{v}'$ is computed so that the final velocity $\boldsymbol{v}^{n+1}$ satisfies the continuity equation. Dropping all but two terms in the corrective part of the momentum equation leads to a relation between the corrective velocity and the corrective part of the pressure $\partial \boldsymbol{v}'/\partial t = -\operatorname{grad} p'$. With the time derivative discretized as an explicit Euler scheme, $\boldsymbol{v}' = -\mathrm{d}t \operatorname{grad} p'$ is obtained. Taking the divergence of this equation and substituting $\operatorname{div} \boldsymbol{v}'$ by $-\mathrm{d}t\nabla^2 p'$ in the continuity equation $\operatorname{div} \boldsymbol{v}^* + \operatorname{div} \boldsymbol{v}' = 0$ results in $\operatorname{div} \boldsymbol{v}^* = \mathrm{d}t\nabla^2 p'$ for a constant time step $\mathrm{d}t$. The velocity at the old time level $\boldsymbol{v}^n$ can be used instead of the provisional velocity $\boldsymbol{v}^*$ without substantially reducing the overall speed of convergence

$$\operatorname{div} \boldsymbol{v}^n = \mathrm{d}t\nabla^2 p' \tag{15}$$

This equation is often called the *pressure-correction equation*. Once this equation is solved for p', the corrective values of the velocity are $\boldsymbol{v}' = -\mathrm{d}t \operatorname{grad} p'$. With the expressions

$$\hat{L}_\eta\big|_{i,j} = (1/J)\left(\eta_x^2 + \eta_y^2 + \eta_z^2\right)\big|_{i,j} \qquad \hat{L}\zeta\big|_{i,j} = (1/J)\left(\zeta_x^2 + \zeta_y^2 + \zeta_z^2\right)\big|_{i,j} \tag{16}$$

a second-order accurate central approximation of the Laplace operator on an orthogonal grid is formed. The pressure-correction equation in semidiscretized form is given by

$$(1/J)\operatorname{div} \boldsymbol{v}^n = Ls_{i-1,j}\, p'_{i-1,j} + Ls_{i,j-1}\, p'_{i,j-1} + Ls_{i+1,j}\, p'_{i+1,j} + Ls_{i,j+1}\, p'_{i,j+1} - Ls_{i,j}\, p'_{i,j} \tag{17}$$

$$Ls_{i\pm1,j} = \tfrac{1}{2}\left[(\mathrm{d}t\hat{L}_\eta)\big|_{i,j} + (\mathrm{d}t\hat{L}_\eta)\big|_{i\pm1,j}\right] \tag{18}$$

$$Ls_{i,j\pm1} = \tfrac{1}{2}\left[(\mathrm{d}t\hat{L}_\zeta)\big|_{i,j} + (\mathrm{d}t\hat{L}_\zeta)\big|_{i,j\pm1}\right] \tag{19}$$

$$Ls_{i,j} = Ls_{i-1,j} + Ls_{i+1,j} + Ls_{i,j-1} + Ls_{i,j+1} \tag{20}$$

The pressure-correction equation does not have to be solved up to machine accuracy at every time step; a few sweeps forward and backward through the domain are enough. The scheme in this form is very similar to the SIMPLE[7] and SIMPLEC[20] schemes. In the present new approach the pressure gradient in the momentum equations and the divergence operator in the continuity are included in the upwind scheme.

E. Fully Coupled Approach

In the fully coupled approach the continuity and the momentum equations are solved together as one system of equations with an implicit solution algorithm. To improve the properties of the resulting linear system of equations, the time derivatives of the unsteady form of the momentum equations are added to the system. This gives rise to an additional term $\partial \boldsymbol{Q}_{\mathrm{APD}}/\partial t$ with $\boldsymbol{Q}_{\mathrm{APD}} = (1/J)[-F_{\mathrm{APD}}\,\mathrm{d}t\nabla^2 p, u, v, w]^T$. For the coupled approach the coefficient F_{APD} is set to a constant. It can be chosen to control stability and convergence of the method. Large values of F_{APD} enhance the stability of the solution procedure but slow down convergence. Numerical experiments suggest the range of values $0.1 \geq F_{\mathrm{APD}} \geq 0$. On writing the right-hand side $\boldsymbol{R}(\boldsymbol{Q})$

$$\boldsymbol{R}(\boldsymbol{Q}) = -\left[\frac{\partial(\boldsymbol{E}_c + \boldsymbol{E}_p)}{\partial \xi} + \frac{\partial(\boldsymbol{F}_c + \boldsymbol{F}_p - \boldsymbol{F}_v)}{\partial \eta} + \frac{\partial(\boldsymbol{G}_c + \boldsymbol{G}_p - \boldsymbol{G}_v)}{\partial \zeta}\right] \tag{21}$$

the system of equations $\boldsymbol{S}(\boldsymbol{Q})$ can be written as $\boldsymbol{S}(\boldsymbol{Q}) = \partial \boldsymbol{Q}_{\mathrm{APD}}/\partial t - \boldsymbol{R}(\boldsymbol{Q}) = 0$, where $\boldsymbol{Q}$ is the vector of the flow variables. The solution at the new iteration level $\boldsymbol{Q}^{n+1}$ is the solution at the old iteration level plus the corrective values $\boldsymbol{Q}^{n+1} = \boldsymbol{Q}^n + \delta \boldsymbol{Q}$. To find the solution at the new iteration level, the system $\boldsymbol{S}(\boldsymbol{Q}^{n+1}) = 0$ is linearized around $\boldsymbol{Q}^n$ to yield

$$\boldsymbol{J}_S(\boldsymbol{Q}^n)\delta \boldsymbol{Q} = \boldsymbol{R}(\boldsymbol{Q}^n) \tag{22}$$

with the Jacobian matrix $\boldsymbol{J}_S(\boldsymbol{Q})$ of the system $\boldsymbol{S}(\boldsymbol{Q})$

$$\boldsymbol{J}_S(\boldsymbol{Q}^n) = \frac{1}{\mathrm{d}t}\frac{\partial \boldsymbol{Q}_{\mathrm{APD}}}{\partial \boldsymbol{Q}} - \frac{\partial \boldsymbol{R}(\boldsymbol{Q}^n)}{\partial \boldsymbol{Q}} \tag{23}$$

Equation (22) is a linear system in $\delta \boldsymbol{Q}$, and it can be solved with a large variety of methods available for linear systems. Repeated iteration is required to find the steady-state solution of Eq. (22) as the momentum equations are nonlinear. For all points of a structured grid in the computational domain, the Jacobian matrix $\boldsymbol{J}_S$ of the system (22) has a banded structure. As approximations used to construct the matrix $\boldsymbol{J}_S$ do not influence the steady-state result, the convective terms are approximated with one-sided first-order differences. The viscous and Poisson terms are approximated with second-order central differences. With this discretization only neighboring points give a contribution, and $\boldsymbol{J}_S$ is of block penta-diagonal structure. The third dimension does not give additional elements in matrix $\boldsymbol{J}_S$, as only one two-dimensional surface is solved at the time:

$$\boldsymbol{J}_S = \left[\boldsymbol{J}_S|_{i,j-1}, 0 \ldots 0, \boldsymbol{J}_S|_{i-1,j}, \boldsymbol{J}_S|_{i,j}, \boldsymbol{J}_S|_{i+1,j}, 0 \ldots 0, \boldsymbol{J}_S|_{i,j+1}\right] \tag{24}$$

The blocks on the diagonals of $\boldsymbol{J}_S$ are, e.g.,

$$\boldsymbol{J}_S|_{i-1,j} = \frac{1}{\mathrm{d}t}\frac{\partial \boldsymbol{Q}_{\mathrm{APD}}|_{i,j}}{\partial \boldsymbol{Q}_{i-1,j}} - \frac{\partial \boldsymbol{R}_{i,j}}{\partial \boldsymbol{Q}_{i-1,j}} \tag{25}$$

The lengthy expressions for $\boldsymbol{J}_S$ are given by Rogers and Kwak[15] and Scholtysik.[32] Artificial compressibility can easily be introduced in the present formulation to increase the diagonal dominance of the system. In addition, the velocity changes can be smoothed by taking a higher viscosity in the viscous contribution to $\boldsymbol{J}_S$.

Following Yoon and Jameson[35] and Yoon and Kwak,[29] the matrix $\boldsymbol{J}_S$ can be approximated as

$$\boldsymbol{J}_S = \boldsymbol{L} - \boldsymbol{D} + \boldsymbol{U} \approx \boldsymbol{L}\boldsymbol{D}^{-1}\boldsymbol{U} \tag{26}$$

where $\boldsymbol{L}$ is the lower triangular part of $\boldsymbol{J}_S$ including the diagonal, $\boldsymbol{D}$ is the diagonal of $\boldsymbol{J}_S$, and $\boldsymbol{U}$ is the upper triangular part including the diagonal. An important aspect of this splitting is that the elements in $\boldsymbol{L}$, $\boldsymbol{D}$, and $\boldsymbol{U}$ are the same as in the original matrix $\boldsymbol{J}_S$ and no decomposition into $\boldsymbol{L}$ and $\boldsymbol{U}$ is needed. Equation (22) can be approximated as

$$\boldsymbol{L}\boldsymbol{D}^{-1}\boldsymbol{U}\delta\boldsymbol{Q} = \boldsymbol{R} \tag{27}$$

The system (27) can be solved in three steps:

$$\delta\boldsymbol{Q}^* = \boldsymbol{L}^{-1}\boldsymbol{R}, \qquad \delta\boldsymbol{Q}^{**} = \boldsymbol{D}\delta\boldsymbol{Q}^*, \qquad \delta\boldsymbol{Q} = \boldsymbol{U}^{-1}\delta\boldsymbol{Q}^{**} \tag{28}$$

This involves the inversion of two triangular matrices, i.e., simple forward and backward substitutions, respectively, and a multiplication of a diagonal matrix with a vector. The algorithm is fully vectorizable along lines $i + j = \text{constant}$.

The splitting can be based either on blocks or on single matrix elements as proposed by Küffer.[36] For the splitting based on elements, the matrix $\boldsymbol{D}$ is a diagonal matrix with single elements as diagonal entries. If the splitting is based on blocks, the inversion of the matrix $\boldsymbol{D}$ involves the inversion of 4×4 blocks on the diagonal of $\boldsymbol{D}$, unless the approximate form of the split Jacobian $\boldsymbol{A}^{\pm}$ is used. Following Yoon et al.,[35] $\boldsymbol{A}^{\pm}$ can be approximated alternatively as $\boldsymbol{A}^{\pm} \approx \frac{1}{2}(\boldsymbol{A} \pm \hat{\rho}_A \boldsymbol{I})$ with $\hat{\rho}_A = \kappa \max(|\lambda_A|)$, where $\hat{\rho}_A$ is the spectral radius of the matrix $\boldsymbol{A}$ times a constant κ, $\boldsymbol{I}$ is a 4×4 identity matrix, and λ_A the eigenvalues as used in the upwind scheme. To compensate the factorization error made in the approximation of the Jacobian matrix $\boldsymbol{J}_S$ [Eq. (26)], the lower-upper symmetric-Gauss–Seidel solver can be repeated iteratively. Two to eight iterations have shown to work well. Underrelaxation can be used to stabilize the iteration by applying only a fraction ω of the computed values $\delta\boldsymbol{Q}$ to update the solution. Numerical experiments suggest ω to be around 0.8 for a fast and robust convergence.

F. Discretization of Inviscid Terms

Inviscid Terms in the Main Flow Direction

The discretization of the inviscid terms in the main flow direction is done with one-sided operators to ensure a stable marching scheme. The convective flux in the main flow direction is discretized as $(\partial \boldsymbol{E}_c/\partial\xi)|_k \approx \boldsymbol{E}_c|_{k+1/2} - \boldsymbol{E}_c|_{k-1/2}$ with the velocity taken from a forward extrapolation $u_{k+1/2} = u_k + \frac{1}{2}(u_k - u_{k-1})$, where k is the index of the crossflow surfaces.

In the SPM the pressure flux in the main flow direction is $\partial \boldsymbol{E}_p/\partial\xi = \partial p_{\mathrm{cl}}/\partial\xi (1/J)\,[0 \;\; \xi_x \;\; \xi_y \;\; \xi_z]^T$, with $\partial p_{\mathrm{cl}}/\partial\xi$ determined during the solution process. In the MPM the pressure flux is discretized in the same manner as the convective fluxes $(\partial \boldsymbol{E}_p/\partial\xi)|_k \approx \boldsymbol{E}_p|_{k+1/2} - \boldsymbol{E}_p|_{k-1/2}$ but with the pressure known from a backward extrapolation $p_{k+1/2} = p_{k+1} - \frac{1}{2}(p_{k+2} - p_{k+1})$.

Upwind Scheme in the Crossflow Directions

The inviscid fluxes in the crossflow directions are approximated for each coordinate direction separately as proposed by Rogers and Kwak.[15] The scheme is described here only briefly for one coordinate direction. An analogous formulation is used for the other crossflow direction. With $\boldsymbol{f} = \boldsymbol{F}_c + \boldsymbol{F}_p$ the derivative of the convective and pressure fluxes at the location i is discretized as $\partial \boldsymbol{f}/\partial\eta|_i \approx (\hat{\boldsymbol{f}}_{i+1/2} - \hat{\boldsymbol{f}}_{i-1/2})/\mathrm{d}\eta$ with $\hat{\boldsymbol{f}}_{i+1/2} = \frac{1}{2}(\boldsymbol{f}_i + \boldsymbol{f}_{i+1} + \Phi_{i+1/2})$. The flux-difference splitting technique is used to derive an upwind scheme. The Jacobian matrix $\boldsymbol{A} = \partial \boldsymbol{f}/\partial \boldsymbol{Q}$ is split into two parts according to the sign of its eigenvalues λ_1 to λ_4

$$\boldsymbol{A}^{\pm} = (1/J)\left(\boldsymbol{X}_A \Lambda_A^{\pm} \boldsymbol{X}_A^{-1}\right)$$

$$\Lambda_A = \mathrm{diag}(V_c,\, V_c,\, V_c + C_A,\, V_c - C_A) \tag{29}$$

$$\Lambda_A^{\pm} = \tfrac{1}{2}(\Lambda_A \pm |\Lambda_A|), \qquad C_A = \sqrt{V_c^2 + \eta_x^2 + \eta_y^2 + \eta_z^2} \tag{30}$$

The expressions for the Jacobian matrix $\boldsymbol{A}$, its split form $\boldsymbol{A}^{\pm}$, and its right and left eigenvectors $\boldsymbol{X}_A$ and $\boldsymbol{X}_A^{-1}$ are given in Rogers and Kwak[15] and adapted to the present formulation in Scholtysik.[32] With $\Delta\boldsymbol{Q}_{i+1/2} = \boldsymbol{Q}_{i+1} - \boldsymbol{Q}_i$ and the matrices $\boldsymbol{A}^{\pm}$, the flux differences are split into $\Delta \boldsymbol{f}^{\pm}_{i+1/2} = \boldsymbol{A}^{\pm}_{i+1/2}\Delta\boldsymbol{Q}_{i+1/2}$. The dissipation term $\Phi_{i+1/2}$ is constructed with $\Delta \boldsymbol{f}^{\pm}$, yielding a scheme of first, third, or fifth order. The fifth-order scheme is given by

$$\Phi_{i+\frac{1}{2}} = \tfrac{1}{30}\Big(-2\Delta \boldsymbol{f}^+_{i-\frac{3}{2}} + 11\Delta \boldsymbol{f}^+_{i-\frac{1}{2}} - 6\Delta \boldsymbol{f}^+_{i+\frac{1}{2}} - 3\Delta \boldsymbol{f}^+_{i+\frac{3}{2}} + 2\Delta \boldsymbol{f}^-_{i+\frac{5}{2}} - 11\Delta \boldsymbol{f}^-_{i+\frac{3}{2}} + 6\Delta \boldsymbol{f}^-_{i+\frac{1}{2}} + 3\Delta \boldsymbol{f}^-_{i-\frac{1}{2}}\Big) \tag{31}$$

G. Local Time Steps

Viscous and inviscid terms pose different restrictions on the time step of an explicit Euler time discretization. The more severe determines the time step $\mathrm{d}t = \min(\mathrm{d}t_{\mathrm{vis}}, \mathrm{d}t_{\mathrm{inv}})$, where

$$\mathrm{d}t_{\mathrm{vis}} \le (Re/2\nu)\left(\eta_x^2 + \eta_y^2 + \eta_z^2 + \zeta_x^2 + \zeta_y^2 + \zeta_z^2\right)^{-1} \tag{32}$$

and the inviscid time step is estimated with the help of the spectral radius from the upwind model as

$$\mathrm{d}t_{\mathrm{inv}} \le \left\{2\left[(|U_c| + C_C)^2 + (|V_c| + C_A)^2 + (|W_c| + C_B)^2\right]\right\}^{-\frac{1}{2}} \tag{33}$$

This formulation of the inviscid time step does not produce infinite values of $\mathrm{d}t_{\mathrm{inv}}$ at points of vanishing velocity. As only the final steady-state solution is required and not the transient evolution, different time steps can be used for different points of a crossflow surface to speed up convergence.

H. Boundary Conditions

At the inflow boundary of the channel, velocity profiles of all three components have to be specified, but no pressure information is needed. At the exit plane of the channel, only the MPM requires a pressure distribution. It is taken from a previous single-pass sweep through the domain.

On solid walls $\boldsymbol{v} = 0$, and a zero pressure gradient normal to the wall surface is imposed. Here, the pressure gradient is discretized with the standard finite difference operator of second-order accuracy. A modified divergence operator has to be used next to the boundary because of the restrictions imposed by the divergence theorem. For any regular vector field $\hat{\boldsymbol{v}}$ it is

$$\iint_{S_{\mathrm{CV}}} \hat{\boldsymbol{v}} \cdot \boldsymbol{n}\,\mathrm{d}S = \iiint_{V_{\mathrm{CV}}} \mathrm{div}\,\hat{\boldsymbol{v}}\,\mathrm{d}V \tag{34}$$

where S_{CV} is the boundary of an arbitrary volume V_{CV} and $\boldsymbol{n}$ the outer unit normal on the surface S_{CV}. Disregarding this condition can lead to nonconvergence of the pressure-correction equation in the segregated approach. Figure 2 shows the regular divergence operator for inner grid points and a modified operator at the boundary.

In the discretized form of Eq. (34), the integral of the divergence in V_{CV} equals the flux over the surface $\hat{S}_{\mathrm{CV}}$, marked with the dotted line in Fig. 2, and not the flux over the original domain S_{CV}, marked

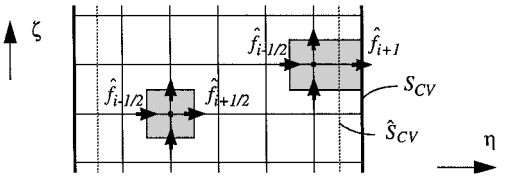

Fig. 2 Divergence operator at the boundary.

with the solid line. To use the known velocities at the original boundary S_{CV}, a modification of the divergence operator is introduced as $\partial f/\partial \eta = \frac{2}{3}(\hat{f}_{i+1} - \hat{f}_{i-1/2})$. At interior points the quantities f and $\hat{f}$ are defined by the upwind scheme. The flux $\hat{f}_{i+1}$ at the boundary is obtained from local quantities at $i+1$ only. If the specified normal velocity at the boundary satisfies $\int_{S_{CV}} \hat{\boldsymbol{v}} \cdot \boldsymbol{n}\, \mathrm{d}S = 0$, the solution will be divergence free in the discrete sense at all interior points. As the velocity at the new iteration step $\boldsymbol{v}^{n+1}$ is known, the corrective velocity $\boldsymbol{v}'$ is zero on the boundary, and the normal derivative of the corrective pressure is $\partial p'/\partial n = 0$.

III. Verification

A. Test Cases for the Two-Dimensional Navier–Stokes Equations

The capabilities of the code to solve the incompressible two-dimensional Navier–Stokes equations are tested on the two-dimensional driven cavity at Reynolds numbers of 100, 1000, and 1.0×10^4. The velocity is zero on all four sides of the physical domain, except on the upper wall where the tangential component v is set to 1.0. The flow is assumed to be laminar. All results presented here are obtained with the fifth-order upwind biased scheme, as it is found to be superior to the third-order scheme, in particular for the case $Re = 1.0 \times 10^4$. Ghia et al.[37] published a detailed computational investigation of the two-dimensional driven-cavity problem. They use a stream-function vorticity method on uniform grids with up to 257×257 points. The results for the three Reynolds numbers are plotted in Fig. 3. Although the cases $Re = 100$ and 1000 were computed with considerably fewer grid points than those of Ghia et al.,[37] very good agreement is obtained for both. The case $Re = 1.0 \times 10^4$ shows small deviations from the reference solution. With the same number of grid points but employing grid clustering, the present method results in slightly higher velocities than the reference, indicating less overall numerical dissipation. A summary of important computational parameters is given in Table 1.

The convergence history in the case $Re = 1000$ is shown in Fig. 4. The execution time refers to a Cray-J90 computer with a single CPU (240 s corresponds to 1000 implicit iterations). The solid line is obtained with the computational parameters as given in Table 1, and the dashed line indicates a reference computation obtained without artificial pressure-diffusion terms ($F_{APD} = 0.0$, $\kappa = 1.0$). A uniform and slightly faster convergence is obtained using the APD terms. Lower values of κ usually resulted in faster convergence but also had a destabilizing effect on the computations. For $\kappa < 1.0$ convergence could not be achieved without APD terms. The dotted line in Fig. 4 was obtained with a relatively large value of $F_{APD} = 0.01$ and κ as low as 0.5 to demonstrate the stabilizing effect of the APD terms. The excellent results obtained for the driven-cavity test case confirm the accuracy of the present method and its validity for nonuniform grids.

B. Grid-Refinement Test

The accuracy of the present scheme is verified by a grid-refinement test. The driven cavity at $Re = 100$ with a uniform grid spacing and with the same mesh size in both directions is used as a test case. The component of the velocity w at the location

Table 1 Computational parameters for driven cavity

Reynolds number	Grid	Grid stretching ($\Delta y_{max}/\Delta y_{min}$)	F_{APD}	Implicit scheme
100	33 × 33	3.0	0.01	Blocks, κ = 0.4
1000	63 × 63	10.0	0.003	Blocks, κ = 0.7
1.0×10^4	127 × 127	10.0	0.001	Blocks, κ = 1.0

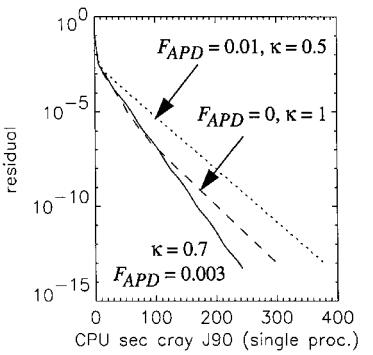

Fig. 4 Convergence history for $Re = 1000$.

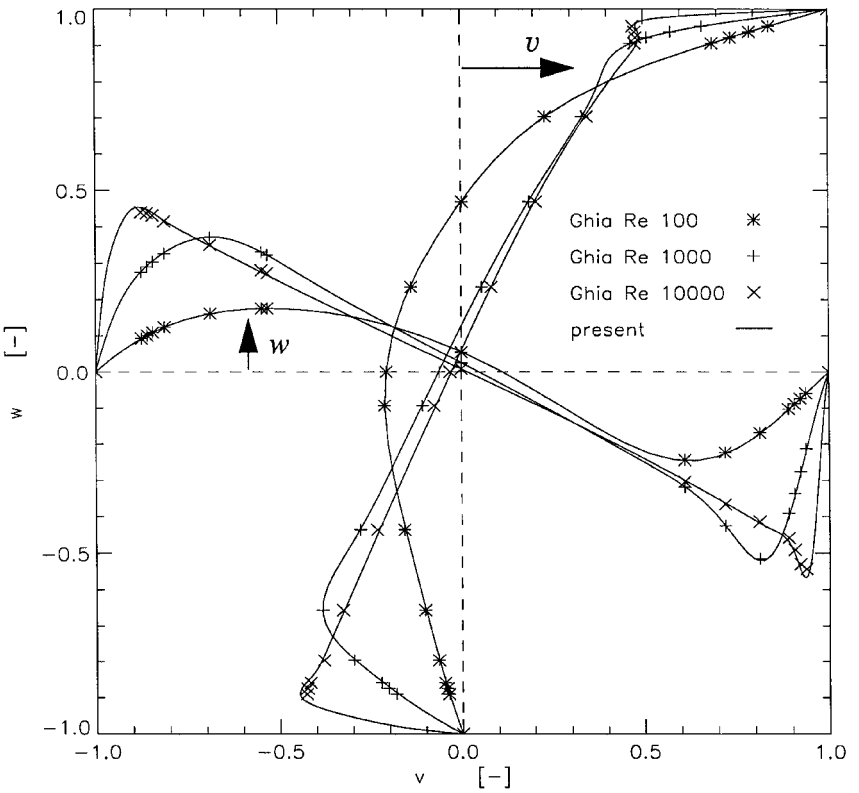

Fig. 3 Velocity profiles on dashed line through the center of the cavity.

$y = 0.25$, $z = 0.5$ is taken as reference value w_{ref}. The values obtained on grids of 17, 33, 65, 129, and 257 grid points (in both directions) are compared to the value (w_{ref0}) obtained from a Richardson extrapolation of the computed values. The reduction of the error $|w_{ref} - w_{ref0}|/w_{ref0}$ is shown in Fig. 5. The dashed line in Fig. 5 corresponds to the reduction rate of a second-order scheme. The results confirm the expected second-order accuracy of the scheme proposed here as the viscous terms are discretized with a scheme of second-order accuracy.

C. Test Cases for the Three-Dimensional Reduced Navier–Stokes Equations

The PNS code is tested on the laminar developing flow in a curved square channel of constant cross section for two different Reynolds and Dean numbers. The geometry of this test case is sketched in Fig. 6. The Reynolds number is formed with the hydraulic diameter l_0 of the channel, the viscosity ν, and the inlet velocity U_{cs}. The Dean number is defined as $De = Re\sqrt{(l_0/R_c)}$, where R_c is the curvature of the channel. The velocities are shown in terms of the scaled contravariant velocity defined as

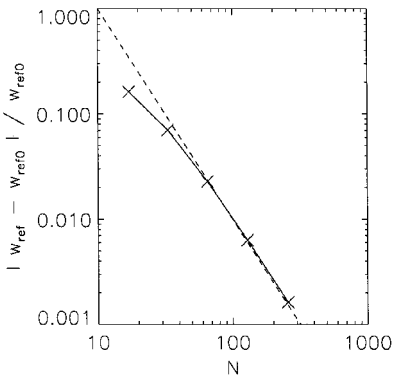

Fig. 5 Grid-refinement test.

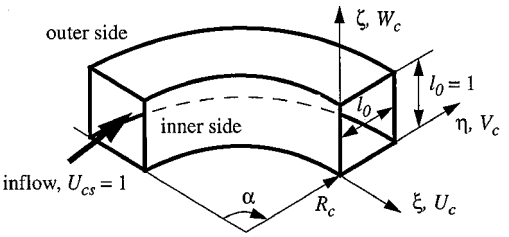

Fig. 6 Geometry of curved square channel with constant cross section.

$$U_{cs} = U_c\Big/\sqrt{\xi_x^2 + \xi_y^2 + \xi_z^2}, \qquad V_{cs} = V_c\Big/\sqrt{\eta_x^2 + \eta_y^2 + \eta_z^2}$$

$$W_{cs} = W_c\Big/\sqrt{\zeta_x^2 + \zeta_y^2 + \zeta_z^2} \tag{35}$$

Starting from a uniform inlet velocity $U_{cs} = 1.0$, a peaked velocity profile develops in the main flow direction together with a secondary crossflow pattern caused by the viscous interaction with the walls and the curvature of the channel. Downstream of the entrance region of the channel, the flow reaches an equilibrium state and does not change any more. Here, the pressure changes only by a constant from one crossflow surface to the next, and the PNS equations are no longer an approximation but exact. Ghia and Sokhey[38] computed this flow for various Reynolds and Dean numbers solving the PNS equations. The low resolution of 21 × 21 grid points on a crossflow surface and 301 points in the main flow direction used in their work is adopted here.

The case $Re = 206$, $De = 55$ shows only one pair of vortices in the crossflow. The velocity component in the main flow direction U_{cs} is shown in Fig. 7 for the fully developed state at $\alpha > 110$ deg. The pressure drop on the centerline is compared to the results of Ghia et al.[38] The present results agree quite well with results of Ghia et al.[38] and those of Aslan.[10] A vector plot of the crossflow and a cut at $\eta = 0.6$ (dashed line) are shown in Fig. 8.

An additional pair of vortices first appears at $De = 143$ according to Ghia et al.[38] Figure 9 shows a vector plot of the crossflow and a profile of V_{cs} on the line $\eta = 0.8$ (dashed line) for the case $Re = 858$. The present results confirm the first appearance of a second pair of vortices at $De = 143$ that demonstrates the minor dissipative effect of the higher-order upwind formulation. These two test cases confirm the ability of the SPM to predict developing three-dimensional flows in slender channels.

IV. BLC

The test section of the BLC is shown in Fig. 1. It is 3 m long and has a flat floor. The rectangular cross sections change from 0.8 m width and 0.25 m height at the right end to 0.4 m width and 0.5 m height at the left end, while the cross section area stays constant. The channel shape corresponds to a stream surface of an analytical potential solution.[1,2] The two-dimensional reference channel is 3.0 m long and 0.8 m wide. The heights of its rectangular cross sections increase linearly from 0.25 to 0.265 m to compensate for the displacement effect of the boundary layer. The results obtained with the present method for the turbulent flow in the BLC are compared with measurements,[1,2] results of a boundary-layer method,[39–41] and results of a compressible thin-layer Navier–Stokes method.[42,43] For the presentation of the results, the Cartesian coordinate system x, y, z is used as in the work of Pompeo.[1] The x axis is oriented along the line of symmetry with $x = 0$ at the location of the first measurements and y the distance from the channel floor. The reference quantities are $l_0 = 1$ m, $v_0 = 42.8$ m/s, and $\nu_0 = 1.711 \times 10^{-5}$ m^2/s,

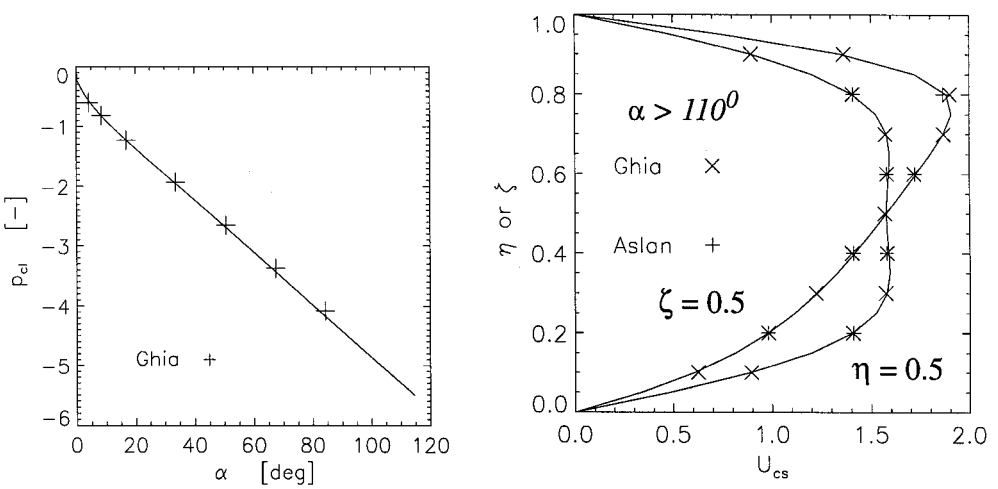

Fig. 7 Centerline pressure and fully developed velocity component in main flow direction ($Re = 206$, $De = 55$).

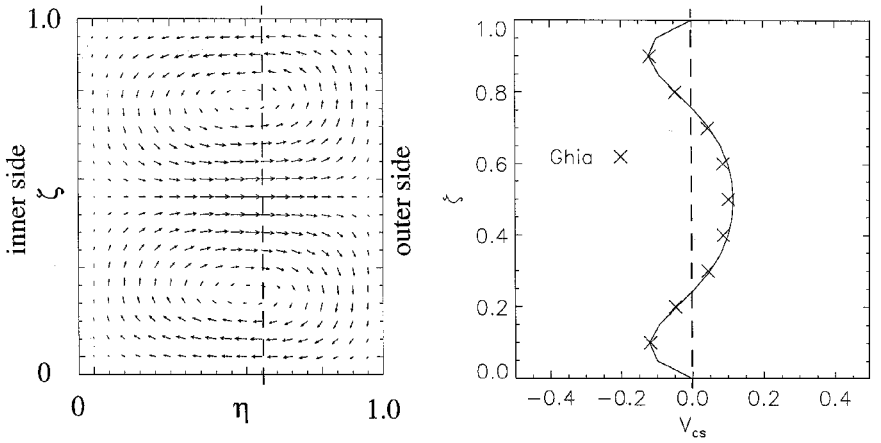

Fig. 8 Vector plot and profile of V_{cs} ($Re = 206$, $De = 55$).

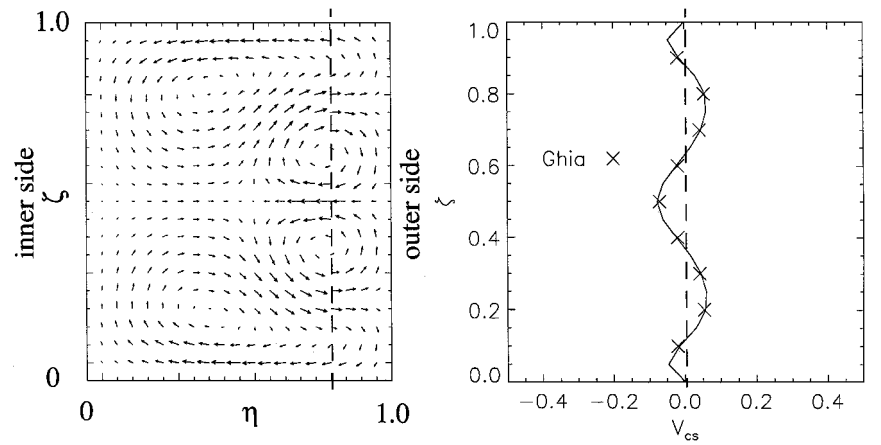

Fig. 9 Vector plot and profile of V_{cs} ($Re = 858$, $De = 143$).

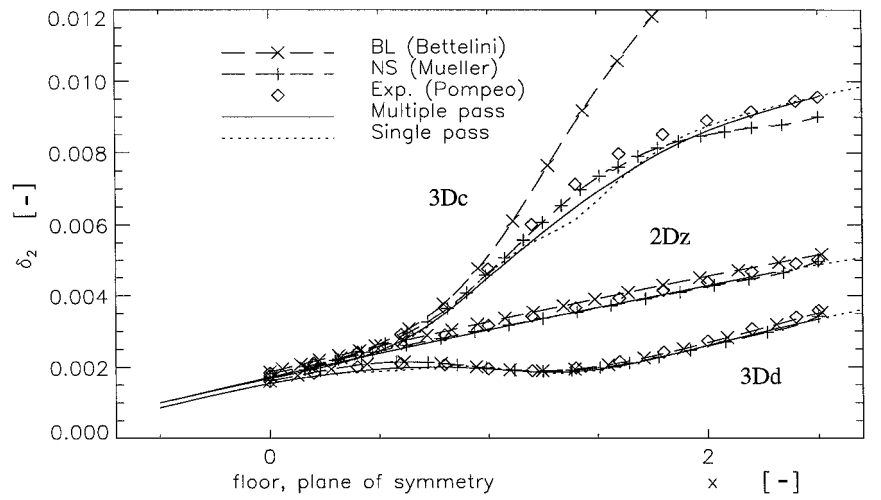

Fig. 10 Momentum thickness along the line of symmetry.

yielding $Re = 2.5 \times 10^6$. The turbulence model of Baldwin and Lomax[31] was used in the present computations and in the reference computations of Müller.[42] The coefficient C_{Cp} of the turbulence model was changed to 1.2 in the computations as proposed by Weisshaar and Reister[44] for incompressible flows. Bettelini et al.[41] use the very similar turbulence model of Cebeci and Smith.[45]

A. Present Method

The inflow boundary conditions were generated with a previous run of the SPM computing a developing, turbulent flow in a straight channel of the same cross section as the nozzle of the BLC. The computation of this virtual channel was stopped when the computed values of the displacement thickness matched the measured quantities. The solution at this position was taken as inflow boundary conditions for the BLC. The ratio of largest to the smallest grid spacing is set to 1600 to keep the first grid point next to the wall at $y^+ \approx 1$. This results in a rather coarse grid in the inviscid core region of the channel although $31 \times 100 \times 80$ grid points are used in x, y, and z directions for one-half of the channel. The computational parameters F_{APD} and κ were set to 0.0003 and 1.1, respectively. A finite time step is not needed to stabilize the implicit system for the applied fully coupled approach. The FLARE[46] approximation had to be used for the case 3Dc, as the streamwise velocity is very low in the upper corners near $x = 1.0$. A thin separation bubble was also

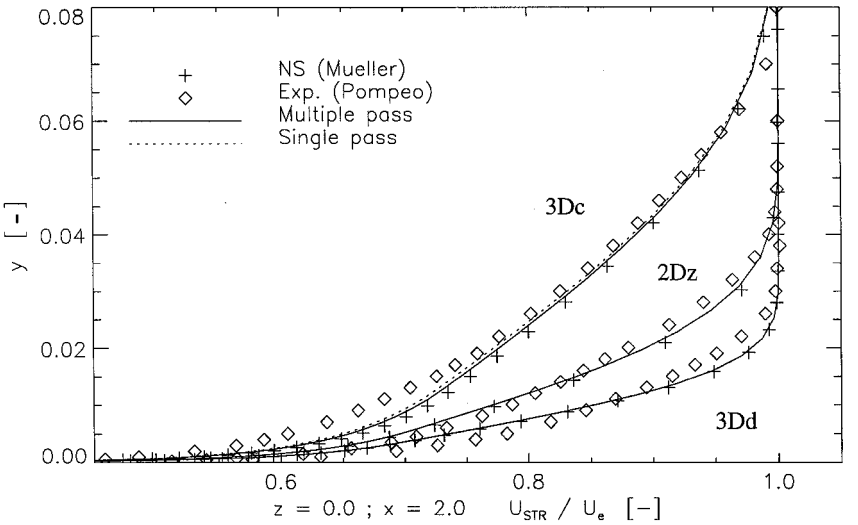

Fig. 11 Streamwise velocity profiles on line of symmetry at $x = 2.0$.

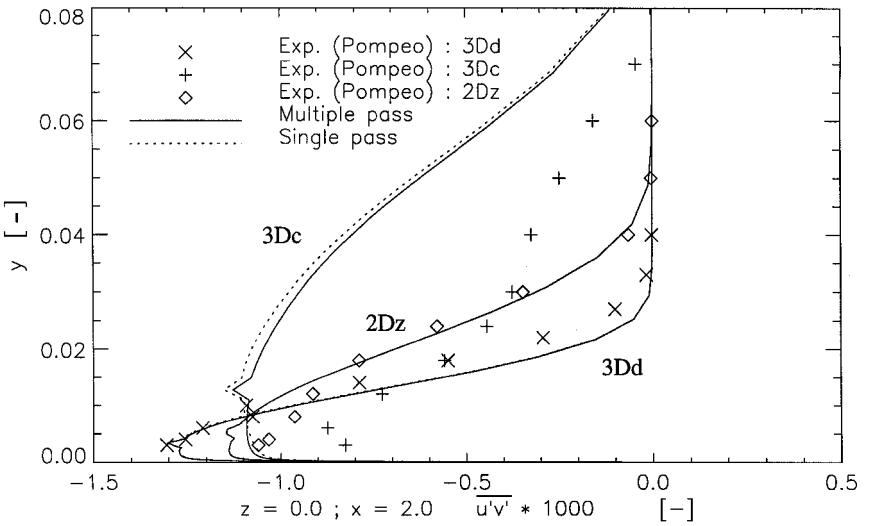

Fig. 12 Reynolds-stress profiles at $x = 2.0$.

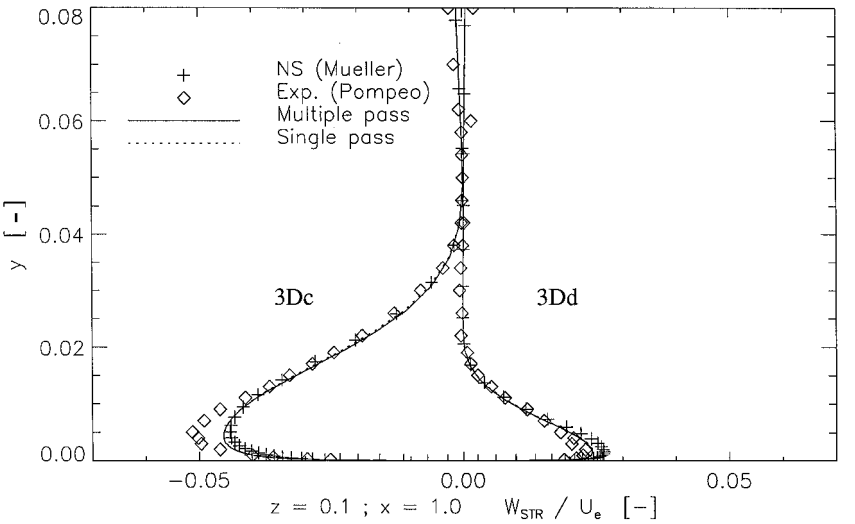

Fig. 13 Crossflow profiles at $x = 1.0$.

found by Müller[42] in this region. Starting with a SPM solution, the MPM needs about 20 iterations for the residual to drop four orders of magnitude on the chosen grid. The pressure field of the potential flow in the nozzle is obtained from the analytical potential solution as given in Pompeo[1] and Pompeo et al.[2]

B. Boundary-Layer Method

This finite difference method described by Bettelini and Fanneløp[40] solves the incompressible, first-order boundary-layer equations in three dimensions written in terms of streamline coordinates. A grid with $300 \times 150 \times 27$ grid points in the x, y, and z directions is used. In comparison with the present and the compressible Navier–Stokes computations, the boundary-layer method allows the best resolution of the floor boundary layer, but the rest of the flow cannot be computed. The case 3Dc shows an unphysical growth of the boundary-layer thicknesses because of a singularity caused by the boundary-layer assumptions for flows with convergent external streamlines as identified by Thomann.[3] Small changes in the boundary conditions can lead to large differences in the solution as shown by Refs. 4, 47, and 48.

C. Compressible Thin-Layer Navier–Stokes Method

Müller[42] uses an implicit second-order upwind finite volume method to solve the compressible Reynolds-averaged thin-layer Navier–Stokes equations on a structured grid. The viscous terms involving streamwise derivatives are neglected. The inviscid fluxes are discretized with the total variation diminishing scheme of Harten and Yee. The ratio of specific heats of air is taken as 1.4, and the (laminar) Prandtl number is assumed to be constant and equal to 0.72. The cases 3Dc and 3Dd are computed on a fine grid with $97 \times 81 \times 50$ grid points in x, y, z directions. A medium grid of $49 \times 41 \times 26$ grid points is used for the case 2Dz. The first grid points next to the floor and roof are at $y^+ \approx 3.5$ for the case 2Dz and at $y^+ \approx 1.5$ for the cases 3Dc and 3Dd. As inflow boundary conditions the streamwise velocity in the turbulent boundary layers can be approximated by Coles profiles using the experimental skin-friction coefficient and streamwise displacement thickness δ_1 of the floor boundary layer. For case 2Dz, $c_f = 0.002953$ and $\delta_1 = 0.01692$ are taken; for case 3Dc, $c_f = 0.003096$ and $\delta_1 = 0.01538$ are taken; and for case 3Dd $c_f = 0.003$ and $\delta_1 = 0.0164$ are taken. In the inviscid core at $x = 0$, the streamwise velocity is constant. The crossflow velocities at $x = 0$ can be set equal to zero.

D. Computational Results

Momentum Thickness Along the Line of Symmetry

Figure 10 shows the streamwise momentum thickness δ_2 along the line of symmetry for the cases 2Dz, 3Dc, and 3Dd. The dotted line denotes the results obtained with the SPM, and the solid line denotes the MPM results. They are compared with the measurements (diamond markers), with the boundary-layer solution ($\times$ markers on broken line), and with the compressible Navier–Stokes solution (+ markers on broken line). The case 2Dz shows good agreement of all methods with the experiments. The SPM and the MPM give almost identical results for the case 2Dz, although the computational effort of the MPM is much higher. This demonstrates the potential of the SPM to predict slender flows efficiently.

The case 3Dd shows small discrepancies of all methods in comparison with the measurements for δ_2. However, the reduction of δ_2 caused by the lateral divergence of the external streamlines is captured by all methods. The case 3Dc reveals larger differences between the solutions. The lateral convergence of the external streamlines leads to an increase of δ_2. The SPM and MPM are able predict this trend; δ_2 is within 15% of the measurements. The MPM shows better agreement than the SPM. The additional errors of the SPM originate from the approximation of the pressure gradient in the streamwise direction and lead to a less accurate prediction of the inviscid core. The compressible Navier–Stokes solution shows good agreement in most parts of the channel, whereas the boundary-layer method fails to predict this case downstream of $x = 1.0$.

Streamwise Velocity Profiles on the Line of Symmetry

The velocity profiles are presented in terms of streamline and crossflow components as in the work of Pompeo et al.[2] as $U_{\text{str}} = \sqrt{(u^2 + w^2)}\cos(\gamma - \gamma_e)$ and $W_{\text{str}} = \sqrt{(u^2 + w^2)}\sin(\gamma - \gamma_e)$, with γ as the angle between the velocity vector and the plane of symmetry. The angle γ_e and the velocity U_e at the boundary-layer edge are used as reference quantities. The streamwise velocity profiles in the turbulent boundary layer above the floor are shown in Fig. 11 for the location $x = 2.0$ on the line of symmetry. For the cases 2Dz and 3Dd the SPM and the MPM give almost identical results, very close to the compressible Navier–Stokes solution. The computed velocity profiles show a lower velocity at the bottom and a higher velocity in the upper regions of the boundary layer as compared to the measurements. For the case 3Dc the discrepancies between the computations and the measurements are more pronounced.

Turbulence Profiles on the Line of Symmetry

The nondimensional Reynolds-stress component $\overline{u'v'}$ as measured by Pompeo[1] is compared with the computed value $-\nu_t\, \mathrm{d}u/\mathrm{d}y$ based on the eddy-viscosity ansatz $\overline{u'v'} = -\nu_t\, \mathrm{d}u/\mathrm{d}y$. The Reynolds-stress profiles at the location $x = 2.0$ are given in Fig. 12. The markers denote the experiments of Pompeo. Both the SPM and the MPM are in fair agreement with the measurements in the cases 2Dz and 3Dd. Large differences, up to a factor of two, are found for the case 3Dc where the Reynolds stress is overpredicted in the upper regions of the boundary layer. However, the maximum value of $|\overline{u'v'}|$ in the profile is predicted quite accurately. According to the measurements and the computations, the Reynolds stress close to the wall is higher in the divergent case and lower in the convergent case. The kinks at the crossover distances, where the inner and outer eddy viscosities intersect, can be avoided by a smooth blend[39] instead of using min $\{(\nu_t)_{\text{inner}}, (\nu_t)_{\text{outer}}\}$.

Crossflow Velocity Profiles off the Symmetry Line

Figure 13 shows the crossflow profiles W_{str} for the cases 3Dc and 3Dd at the location $x = 1.0$ off the symmetry line at $z = 0.1$. The magnitude of the crossflow velocity is only about 5% of the streamwise velocity. The crossflow of the case 3Dc and of the case 3Dd have different signs. The SPM and the MPM give almost identical results very similar to the compressible Navier–Stokes results. In the case 3Dc the crossflow velocity is underpredicted by about 10%.

Grid Sensitivity of the Results

The accurate prediction of the turbulent quantities requires the laminar sublayer to be resolved by several grid points. The grid stretching is chosen to keep the first grid point at $y^+ \approx 1.0$. Grid-refinement tests revealed a grid dependence of the solution with the resolution presently chosen. Introducing a finer grid spacing close to the wall changed the quantities at the wall by a few percent without altering the character of the solution. Four times as many grid points in the x direction gave results almost identical with those obtained with the original grid.

V. Conclusions

A space-marching method designed to solve the reduced forms of the three-dimensional steady Navier–Stokes equations for internal incompressible flows has been developed. For slender flows the SPM has shown to be very efficient in terms of computer memory requirements and execution time. It produces accurate solutions very close to the thin-layer Navier–Stokes solution at a fraction of the effort. Compared to boundary-layer methods, the SPM computes the flow in the entire channel including the corners and not only in a limited region of dependence. So-called departure solutions or nonconvergence of the scheme have not been experienced with the present method. For flows with one predominant flow direction but significant elliptic effects in the pressure field, the MPM can improve the solution found by the SPM. Sweeping against the main flow direction speeds up the overall convergence considerably. The SPM is at least five times faster than the MPM.

The new APD scheme is capable of solving the two-dimensional incompressible steady Navier–Stokes equations as well as the reduced three-dimensional form. No source term is needed in the continuity equation, and no staggered grid or additional pressure and momentum interpolation are necessary to stabilize the solution. Grid-scale oscillations of the dependent variables have not been

observed with the present scheme. The computer memory requirements for the segregated approach are much lower than for the fully coupled approach as the whole task is split into two computationally independent operations. The additional dissipation introduced by the Laplace operator contributes to stabilize the solution process and speeds up convergence. Pressure waves sometimes observed in artificial compressibility computations during the transient phase should be damped to a certain extent. Existing artificial compressibility codes can easily be extended to an APD method by the introduction of the additional APD terms.

The code was developed in FORTRAN77 to run on a Cray-YMP vector computer where it achieved an average speed of 160 Mflops. On the parallel vector computer of Cray-J90 type, it showed the expected speed up for up to four processors. The MPM allows an alternative way of parallelization. The computational domain can be divided into subdomains, located one behind the next. For each subdomain the code can be run independently. As only the data at one crossflow surface have to be kept in memory for each subdomain, the total amount of memory required is still moderate.

The new computer program was tested against established numerical solutions, and excellent results have been achieved. The laminar flow in the two-dimensional driven square cavity at Reynolds numbers from 100 to 1.0×10^4 shows very good agreement with other computations found in the literature. The fifth-order upwind scheme is clearly superior to the low-order schemes often used in connection with the classical pressure-correction schemes and constitutes a good compromise between accuracy and robustness.

The cases 2Dz and 3Dd of the flow in the BLC of the ETH Zürich are predicted with reasonable accuracy, but the case of convergent external streamlines 3Dc reveals some differences between the computations and the measurements, especially toward the end of the nozzle. These differences are caused in large measure by the simple algebraic turbulence model originally developed for two-dimensional flows. For the cases 2Dz and 3Dd the growth rate of the momentum thickness is predicted accurately by all methods, but the velocity in the streamwise direction is too high in the upper part of the boundary layer and too low in the lower part. The absolute value of the Reynolds-stress component $\overline{u'v'}$ in the upper part of the boundary layer is too low in the case 3Dd and much too high in the case 3Dc. For the three-dimensional cases the inviscid core of the flow is predicted less accurately by the SPM than by the MPM because of the approximation of the streamwise pressure gradient. The BLC is designed to produce a vanishing or small pressure gradient in the streamwise direction along the line of symmetry on the floor of the nozzle. However, the other locations in a given cross section are exposed to important pressure gradients, curvature, and convergence/divergence of the streamlines. Uncertainties introduced by the turbulence model in these regions will influence the external velocity and hence all results of the floor boundary layer.

Acknowledgments

The present work was carried out at the Institute of Fluid Dynamics of the Swiss Federal Institute of Technology (ETH Zürich). The availability of the excellent resources of the ETH, especially the supercomputing facilities and well-equipped library, have greatly contributed to this work. We gratefully acknowledge the financial support. Appreciation is also expressed to H. H. Thomann and G. Yadigaroglu for their substantial input.

References

[1]Pompeo, L., "An Experimental Study of Three-Dimensional Turbulent Boundary Layers," Ph.D. Dissertation, Swiss Federal Inst. of Technology, No. 9780, Zurich, 1992.

[2]Pompeo, L., Bettelini, M. S. G., and Thomann, H., "Laterally Strained Turbulent Boundary-Layers Near a Plane of Symmetry," *Journal of Fluid Mechanics*, Vol. 257, 1993, pp. 507–532.

[3]Thomann, H., "Diverging Solutions of the Boundary-Layer Equations Near a Plane of Symmetry," *AIAA Journal*, Vol. 32, No. 9, 1994, pp. 1923–1925.

[4]Scholtysik, M., Bettelini, M. S. G., and Fanneløp, T. K., "A Note on Problems in 3D Boundary Layer Computations in Streamline Coordinates," *Zeitschrift für Angewandte Mathematik und Physik*, Vol. 45, 1994, pp. 153–165.

[5]Anderson, D. A., Tannehill, J. C., and Pletcher, R. H., *Computational Fluid Mechanics and Heat Transfer*, 1st ed., Hemisphere, New York, 1984; also 2nd ed., Taylor and Francis, Washington, DC, 1997.

[6]Kirtley, K. R., and Lakshminarayana, B., "A Multiple Pass Space-Marching Method for Three-Dimensional Incompressible Viscous Flow," *Zeitschrift für Flugwissenschaften und Weltraumforschung*, Vol. 16, 1992, pp. 49–59.

[7]Patankar, S. V., and Spalding, D. B., "A Calculation Procedure for Heat, Mass and Momentum Transfer in Three-Dimensional Parabolic Flows," *International Journal of Heat and Mass Transfer*, Vol. 15, 1972, pp. 1787–1806.

[8]Briley, W. R., "Numerical Method for Predicting Three-Dimensional Steady Viscous Flow in Ducts," *Journal of Computational Physics*, Vol. 14, 1974, pp. 8–28.

[9]Briley, W. R., and McDonald, H., "Three-Dimensional Viscous Flows with Large Secondary Velocity," *Journal of Fluid Mechanics*, Vol. 144, 1984, pp. 47–77.

[10]Aslan, A. R., "Numerical Prediction of Three-Dimensional Subsonic Flow in Ducts Using the Parabolized Navier–Stokes Approach," Ph.D. Dissertation, Faculté des Sciences Appliquées, Inst. von Kármán de Dynamique des Fluides, Univ. Libre de Bruxelles, Brussels, April 1991.

[11]Rubin, S. G., and Tannehill, J. C., "Parabolized/Reduced Navier–Stokes Computational Techniques," *Annual Review of Fluid Mechanics*, Vol. 24, 1992, pp. 117–144.

[12]Fletcher, C. A. J., *Computational Techniques for Fluid Dynamics*, Vol. 2, Springer-Verlag, Berlin, 1991.

[13]Hirsch, C., *Numerical Computation of Internal and External Flows*, Vol. 1, Wiley, New York, 1990.

[14]Chorin, A. J., "A Numerical Method for Solving Incompressible Viscous Flow Problems," *Journal of Computational Physics*, Vol. 2, 1967, pp. 12–26.

[15]Rogers, S. E., and Kwak, D., "Upwind Differencing Scheme for the Time-Accurate Incompressible Navier–Stokes Equations," *AIAA Journal*, Vol. 28, No. 2, 1990, pp. 253–262.

[16]Abdallah, S., "Numerical Solutions for the Pressure Poisson Equation with Neumann Boundary Conditions Using a Non-Staggered Grid, I," *Journal of Computational Physics*, Vol. 70, 1987, pp. 182–192.

[17]Abdallah, S., "Numerical Solutions for the Incompressible Navier–Stokes Equations in Primitive Variables Using a Non-Staggered Grid, II," *Journal of Computational Physics*, Vol. 70, 1987, pp. 193–202.

[18]Sotiropoulos, F., and Abdallah, S., "A Primitive Variable Method for the Solution of Three-Dimensional Incompressible Viscous Flows," *Journal of Computational Physics*, Vol. 103, 1992, pp. 336–349.

[19]Dick, E., "A Flux-Vector Splitting Method for Steady Navier–Stokes Equations," *International Journal for Numerical Methods in Fluids*, Vol. 8, 1988, pp. 317–326.

[20]Van Doormaal, J. P., and Raithby, G. D., "Enhancements of the SIMPLE Method for Predicting Incompressible Fluid Flows," *Numerical Heat Transfer*, Vol. 7, 1984, pp. 147–163.

[21]Patankar, S. V., *Numerical Heat Transfer and Fluid Flow*, Hemisphere, New York 1980.

[22]Raithby, G. D., and Schneider, G. E., "Numerical Solution of Problems in Incompressible Fluid Flow: Treatment of the Velocity-Pressure Coupling," *Numerical Heat Transfer*, Vol. 2, No. 2, 1979, pp. 417–440.

[23]Rodi, W., Majumdar, S., and Schönung, B., "Finite Volume Methods for Two-Dimensional Incompressible Flows with Complex Boundaries," *Computer Methods in Applied Mechanics and Engineering*, Vol. 75, 1989, pp. 369–392.

[24]Gunzburger, M. D., and Nicolaides, R. A., *Incompressible Computational Fluid Dynamics*, Cambridge Univ. Press, Cambridge, England, U.K., 1993.

[25]Rhie, C. M., and Chow, W. L., "Numerical Study of the Turbulent Flow Past an Airfoil with Trailing Edge Separation," *AIAA Journal*, Vol. 21, No. 11, 1983, pp. 1525–1532.

[26]Peric, M., Kessler, R., and Scheuerer, G., "Comparison of Finite-Volume Numerical Methods with Staggered and Collocated Grids," *Computers and Fluids*, Vol. 16, No. 4, 1988, pp. 389–403.

[27]Majumdar, S., Rodi, W., and Zhu, J., "Three-Dimensional Finite-Volume Method for Incompressible Flows with Complex Boundaries," *Transactions of the ASME*, Vol. 114, 1992, pp. 496–503.

[28]Hayase, T., Humphrey, J. A. C., and Greif, R., "A Consistently Formulated QUICK Scheme for Fast and Stable Convergence Using Finite-Volume Iterative Calculation Procedures," *Journal of Computational Physics*, Vol. 98, 1992, pp. 108–118.

[29]Yoon, S., and Kwak, D., "Three-Dimensional Incompressible Navier–Stokes Solver Using Lower-Upper Symmetric-Gauss-Seidel Algorithm," *AIAA Journal*, Vol. 29, No. 6, 1991, pp. 874, 875.

[30]Tafti, D., "Alternate Formulations for the Pressure Equation Laplacian on a Collocated Grid for Solving the Unsteady Incompressible Navier–Stokes Equations," *Journal of Computational Physics*, Vol. 116, No. 1, 1995, pp. 143–153.

[31] Baldwin, B. S., and Lomax, H., "Thin Layer-Approximation and Algebraic Model for Separated Turbulent Flows," AIAA Paper 78-257, 1978.

[32] Scholtysik, M., "On the Solution of a Reduced Form of the Navier–Stokes Equations (PNS) for Internal Incompressible Flows," Ph.D. Dissertation, Swiss Federal Inst. of Technology, No. 11891, Zurich, Oct. 1996.

[33] Pulliam, T. H., and Steger, J. L., "On Implicit Finite-Difference Simulations of Three-Dimensional Flow," AIAA Paper 78-10, Jan. 1978.

[34] Rannacher, R., "On Chorin's Projection Method for the Incompressible Navier–Stokes Equations," *The Navier–Stokes Equations II—Theory and Numerical Methods*, edited by J. G. Heywood, Springer-Verlag, Berlin, 1992, pp. 167–183.

[35] Yoon, S., and Jameson, A., "Lower-Upper Symmetric-Gauss-Seidel Method for the Euler and Navier–Stokes Equations," *AIAA Journal*, Vol. 26, No. 9, 1988, pp. 1025, 1026.

[36] Küffer, J., "Fast Implicit Solvers for the Incompressible Navier–Stokes Equations," *Computational Fluid Dynamics '92: Proceedings of the 1st ECCOMAS CFD Conference*, edited by C. Hirsch, J. Periaux, and W. Kordulla, Elsevier, Amsterdam, 1992.

[37] Ghia, U., Ghia, K. N., and Shin, C. T., "High-Re Solutions for Incompressible Flow Using the Navier–Stokes Equations and a Multigrid Method," *Journal of Computational Physics*, Vol. 48, 1982, pp. 387–411.

[38] Ghia, K. N., and Sokhey, J. S., "Laminar Incompressible Viscous Flow in Curved Ducts of Regular Cross-Sections," *Journal of Fluids Engineering*, Vol. 99, Series 1, No. 4, 1977, pp. 640–648.

[39] Bettelini, M. S. G., "Numerical Study of Some Engineering Turbulence Models for Three-Dimensional Boundary Layers," Ph.D. Dissertation, Swiss Federal Inst. of Technology, No. 9182, Zürich, 1990.

[40] Bettelini, M. S. G., and Fanneløp, T. K., "A Systematic Comparison of Mathematically Simple Turbulence Models for Three-Dimensional Boundary-Layers," *AIAA Journal*, Vol. 31, No. 6, 1993, pp. 999–1006.

[41] Bettelini, M. S. G., Fanneløp, T. K., Scholtysik, M., and Thomann, H., "ETH Test Cases: Experiences with a Boundary-Layer Approach," *Proceedings of the EUROVISC Workshop on Turbulent Boundary Layers in Three Dimensions*, edited by D. Humphreys (to be published).

[42] Müller, B., "Navier–Stokes Simulation of Subsonic Turbulent Flow Through a Wind Tunnel Test Section," *Computational Fluid Dynamics '94: Proceedings of the 2nd ECCOMAS CFD Conference*, edited by S. Wagner, E. H. Hirschel, J. Periaux, and R. Piva, Wiley, Chichester, England, U.K., 1994, pp. 857–863.

[43] Müller, B., "Navier-Stokes Simulation of Turbulent Flow in the Test Section of the ETH Boundary-Layer Wind Tunnel," *Proceedings of the EUROVISC Workshop on Turbulent Boundary Layers in Three Dimensions*, edited by D. Humphreys (to be published).

[44] Weisshaar, E., and Reister, H., "Test und Vergleich von Turbulenzmodellen für die Grenzschicht- und Navier–Stokes Gleichungen," Interner Bericht 221-84 A 12, DFVLR-AVA, Göttingen, Germany, 1984.

[45] Cebeci, T., and Smith, A. M. O., "A Finite-Difference Solution of the Incompressible Turbulent Boundary-Layer Equations by an Eddy-Viscosity Model," *AFOSR-IFP-Stanford Conference on Computation of Turbulent Boundary Layers*, edited by S. J. Klein et al., Stanford Univ., 1968.

[46] Reyhner, T. A., and Flügge-Lotz, I., "The Interaction of a Shock Wave with a Laminar Boundary Layer," *International Journal of Non-Linear Mechanics*, Vol. 3, No. 2, 1968, pp.173–199.

[47] Scholtysik, M., "Berechnung einer Turbulenten 3D Grenzschicht mit konvergenten Aussenstromlinien," Interne Berichte aus dem Institut für Fluiddynamik No. 4, Zurich, Sept. 1993.

[48] Scholtysik, M., and Fanneløp, T. K., "Solution of a Reduced Form of the Navier–Stokes Equations (PNS) for Internal Incompressible Flows," *Proceedings of the EUROVISC Workshop on Turbulent Boundary Layers in Three Dimensions*, edited by D. Humphreys (to be published).

J. Kallinderis
Associate Editor